NATURAL CONVECTION AIR FLOW IN VERTICAL UPRIGHT-ANGLED TRIANGULAR CAVITIES UNDER REALISTIC THERMAL BOUNDARY CONDITIONS

by

Jaime SIERES [a,*], Antonio CAMPO [b], and Jose Antonio MARTINEZ-SUAREZ [a]

[a] Department of Mechanical Engineering, Heat Engines and Machines, and Fluids, School of Industrial Engineering, University of Vigo, Vigo, Spain
[b] Department of Mechanical Engineering, University of Texas, San Antonio, Tex., USA

Original scientific paper
DOI: 10.2298/TSCI130530018S

This paper presents an analytical and numerical computation of laminar natural convection in a collection of vertical upright-angled triangular cavities filled with air. The vertical wall is heated with a uniform heat flux; the inclined wall is cooled with a uniform temperature; while the upper horizontal wall is assumed thermally insulated. The defining aperture angle φ is located at the lower vertex between the vertical and inclined walls.

The finite element method is implemented to perform the computational analysis of the conservation equations for three aperture angles φ = 15º, 30º, and 45º and height-based modified Rayleigh numbers ranging from a low Ra = 0 (pure conduction) to a high 10^9. Numerical results are reported for the velocity and temperature fields as well as the Nusselt numbers at the heated vertical wall. The numerical computations are also focused on the determination of the value of the maximum or critical temperature along the hot vertical wall and its dependence with the modified Rayleigh number and the aperture angle.

Key words: *natural convection, laminar flow, upright-angled triangular cavity, steady-state, finite element method*

Introduction

Buoyancy induced flows inside enclosures is an active research field due to its practical application in nature, science and engineering. The basic topics of the subject are usually covered in any undergraduate heat transfer book [1, 2] and state-of-the-art reviews are usually included in chapters of specialized handbooks [3, 4]. In general, natural convection studies inside enclosures are classified in two main groups: rectangular and non-rectangular enclosures. Despite that a large body of literature exists that describe and analyze fluid flow and heat transfer inside rectangular cavities, non-rectangular enclosures are also considered of prime interest due to its plethora of applications. In particular, triangle shaped enclosures are encountered in many engineering applications such as natural convection in house and buildings attics, solar collectors, electronic equipment, *etc*.

* Corresponding author; e-mail: jsieres@uvigo.es

There are numerous theoretical, numerical and experimental studies in the open literature devoted to natural convection inside triangular cavities with different orientations and various thermal boundary conditions either for laminar or turbulent regimes [5-11]. Although the impact of thermal boundary conditions has been examined, most researches have focused on the consideration of prescribed uniform temperatures and insulation at selected walls of the triangular cavity. Normally, one of the walls is modeled as a hot wall with uniform temperature, facing a cold wall with uniform temperature and the remaining walls are assumed to be thermally insulated.

The case of natural convection from heated vertical walls in a triangular cavity is of special interest due to its direct application in electronics cooling [12-14], where air has been and continues to be the most widely used working fluid for heat rejection [14]. In fact, a configuration of relevance to the electronic industry consists of a heated vertical wall being part of a square or rectangular cavity [12, 13], where heat exchange by natural convection takes place between the heated vertical wall and the opposite cold wall or between the heated vertical wall and an adjacent cold wall [9]. However, in this type of configurations it is clear that natural convection cooling does not provide a constant-temperature bath along the heated vertical wall, producing the appearance of *hot spots* which if not properly managed, may exceed critical temperatures affecting adversely the performance and reliability of electronic components. Therefore, a more realistic analysis would be envisioned if the hot wall is modeled as a uniformly heated wall instead of an isothermal hot wall. Obviously, in these situations an uneven temperature profile emerges along the hot wall. Knowledge of the value and location of the maximum or critical temperature along the hot vertical wall is crucial for a correct design of the heat rejection mechanism in these components.

This paper addresses an analytical and numerical computation of laminar natural convection in vertical upright-angled triangular cavities filled with air. Its peculiarity revolves around a combination of thermal boundary conditions. This configuration may find application in the miniaturization of electronic packaging subjected to space and/or weight constraints, as stated by Simons *et al*. [12] and Bar-Cohen *et al*. [13]. In this work, the vertical wall is uniformly heated with a prescribed heat flux, a prescribed cold temperature is assigned at the inclined wall, while the upper horizontal wall is assumed thermally insulated. The numerical solutions of the Navier-Stokes and energy equations are obtained with the implementation of the finite element method in a suitable computational grid. Numerical results are obtained for the velocity and temperature fields as well as the Nusselt numbers at the heated vertical wall for different values of the height-based Rayleigh number and aperture angles. Two different Nusselt numbers are determined: the first is based on the maximum temperature along the heated vertical wall, whereas the second one is based on the mean temperature along the vertical wall. Knowledge of the Nusselt number as a function of the Rayleigh number and aperture angle will allow analysts to estimate the maximum or critical temperature along the heated vertical wall.

Physical system and mathematical model

The physical system to be considered is sketched in fig. 1. It consists of air confined to a vertically-oriented right-angled triangular cavity made with three impermeable walls. The aperture angle, φ, identifies the bottom vertex of the triangular cavity. A uniform heat flux, q_{H}, is imposed at the vertical wall of length, L_H, the inclined wall of length, L_C, is maintained at a uniform cold temperature, T_C, while the upper connecting horizontal wall of length, L_A, is thermally insulated.

Owing that the dimension perpendicular to the plane of the diagram is long compared to the triangular cavity dimensions, the air motion is conceived to be laminar and 2-D. Because the gravitational acceleration, g, acts parallel to the vertical wall, the buoyant air convection may be modeled by the following system of steady conservation equations:

– mass conservation

$$\frac{\partial u_x}{\partial x}+\frac{\partial u_y}{\partial y}=0 \tag{1}$$

– horizontal momentum and vertical momentum

$$\rho u_x\frac{\partial u_x}{\partial x}+\rho u_y\frac{\partial u_x}{\partial y}=-\frac{\partial p}{\partial x}+\mu\frac{\partial^2 u_x}{\partial x^2}+\mu\frac{\partial^2 u_x}{\partial y^2} \tag{2}$$

$$\rho u_x\frac{\partial u_y}{\partial x}+\rho u_y\frac{\partial u_y}{\partial y}=-\frac{\partial p}{\partial y}+\mu\frac{\partial^2 u_y}{\partial x^2}+\mu\frac{\partial^2 u_y}{\partial y^2}-\rho g\beta\left(T-T_C\right) \tag{3}$$

− energy conservation

$$u_x\frac{\partial T}{\partial x}+u_y\frac{\partial T}{\partial y}=\alpha\frac{\partial^2 T}{\partial x^2}+\alpha\frac{\partial^2 T}{\partial y^2} \tag{4}$$

In the preceding equations, the Boussinesq approximation is invoked, where, ρ, denotes a reference density evaluated at the cold temperature of the inclined wall, T_C. Additionally, the physical properties of the fluid are assumed to be temperature-invariant and $\beta = 1/T_C$ is the coefficient of volumetric thermal expansion.

Assuming that the trapped air does not slip at the cavity walls, the velocity boundary conditions are $u_x = u_y = 0$. The thermal boundary conditions refer to a prescribed low temperature, T_C, at the inclined wall and a prescribed uniform heat flux, q_H, at the vertical wall. At the top horizontal wall, the heat flux is zero to comply with a thermally insulated condition, namely $\partial T/\partial y = 0$.

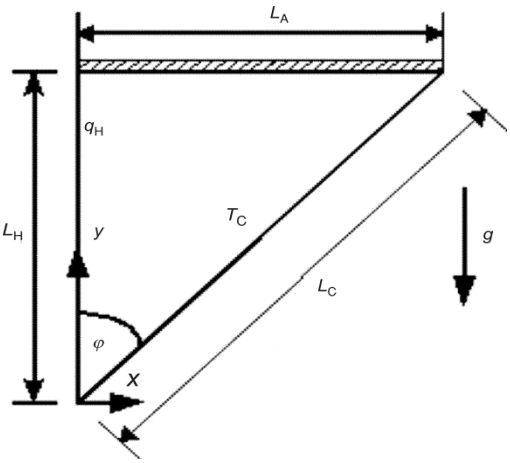

Figure 1. Sketch of the upright right-angled triangular cavity

For convenience, the system of coupled conservation equations is expressed in terms of suitable dimensionless variables. In order to accomplish this, it is necessary to introduce a characteristic velocity, which can be obtained from the kinetic energy gained by the fluid as a result of the work done by the buoyancy forces. A measure of the buoyancy forces per unit volume within the cavity is given by $g\beta\rho\Delta T$, where ΔT stands for the existing temperature difference in the fluid. The buoyancy forces do work on the fluid as it flows inside the cavity. Therefore, a measure of the work done on the fluid can be obtained as the product of the buoyancy forces and a measure of the distance over which these forces act, *i. e.* a characteristic size of the cavity. In this paper, the cavity height, L_H, is considered as the characteristic length of the cavity. Thereby, equating the magnitude of the work done by the buoyancy forces and the kinetic energy gained by the fluid, leads to:

$$g\beta\rho\Delta T L_H = \frac{1}{2}\rho V_c^2 \tag{5}$$

The majority of natural convection problems can be classified in one of the two broad categories:

– external flow around objetcs where the surface temperature, T_w, and ambient temperature, T_∞, are given as input parameters. In these cases a figure of merit refers to a temperature difference in the flow given by $\Delta T = T_w - T_\infty$, and
– internal flow that occurs within enclosed regions where prescribed uniform hot, T_H, and prescribed uniform cold, T_C, temperatures are specified along some of the walls. Then, a figure of merit refers to a temperature difference in the flow given by $\Delta T = T_H - T_C$.

In contrast, in the problem under consideration here, a uniform cold temperature, T_C, is prescribed along the inclined wall and a uniform heat flux, q_H, is prescribed along the vertical wall. In this case, the vertical wall temperature increases with height, and is expected to reach a maximum at the upper edge of the wall. In order to quantify the temperature changes in the flow, the heat flux at the vertical wall is related with fluid temperature field by virtue of the Fourier´s law:

$$q_H = -k\frac{\partial T}{\partial x} \tag{6}$$

The order of magnitude of the temperature gradient within the fluid along the vertical co-ordinate stipulates that:

$$\frac{\partial T}{\partial x} \sim \frac{T_C - T_w}{L_y} \tag{7}$$

where T_w is the temperature of the vertical wall at the vertical position y and L_y – the horizontal distance from the vertical wall to the inclined wall at position y. As a result, the temperature along the vertical wall is supposed to increase with the vertical position, resulting in a maximum, which is located at the upper corner of the cavity. Then, the order of the temperature changes existing in the flow produces:

$$\Delta T = T_{w,max} - T_C \sim \frac{q_H L_A}{k} \tag{8}$$

Combining eqs. (5) to (8), the magnitude of the characteristic velocity of the flow is quantified:

$$V_c = \sqrt{\frac{2g\beta q_H L_H L_A}{k}} \tag{9}$$

For convenience, we drop the factor 2 from the square root and also replace $L_A \sim L_H$, to obtain the following approximate expression for the characteristic velocity:

$$V_c = \sqrt{\frac{g\beta q_H L_H^2}{k}} \tag{10}$$

In view of this, the governing equations can be non-dimensionalized by employing the characteristic velocity, V_c, as the scaled velocity, giving way to the following set of dimensionless variables:

$$X = \frac{x}{L_H}, \quad Y = \frac{y}{L_H} \tag{11}$$

$$U_X = \frac{u_x}{V_c}, \quad U_Y = \frac{u_y}{V_c} \tag{12}$$

$$\theta = \frac{T - T_C}{\Delta T} = k\frac{T - T_C}{q_H L_H}, \quad P = \frac{p}{\rho V_c^2} \tag{13}$$

Correspondingly, the transformed system of steady coupled conservation equations is re-written:

– mass conservation

$$\frac{\partial U_X}{\partial X} + \frac{\partial U_Y}{\partial Y} = 0 \tag{14}$$

– horizontal momentum

$$U_X \frac{\partial U_X}{\partial X} + U_Y \frac{\partial U_X}{\partial Y} = -\frac{\partial P}{\partial X} + \frac{\sqrt{\mathrm{Pr}}}{\sqrt{\mathrm{Ra}}}\left(\frac{\partial^2 U_X}{\partial X^2} + \frac{\partial^2 U_X}{\partial Y^2}\right) \tag{15}$$

– vertical momentum

$$U_X \frac{\partial U_Y}{\partial X} + U_Y \frac{\partial U_Y}{\partial Y} = -\frac{\partial P}{\partial Y} + \frac{\sqrt{\mathrm{Pr}}}{\sqrt{\mathrm{Ra}}}\left(\frac{\partial^2 U_Y}{\partial X^2} + \frac{\partial^2 U_Y}{\partial Y^2}\right) - \theta \tag{16}$$

– energy conservation

$$U_X \frac{\partial \theta}{\partial X} + U_Y \frac{\partial \theta}{\partial Y} = \frac{1}{\sqrt{\mathrm{PrRa}}}\left(\frac{\partial^2 \theta}{\partial X^2} + \frac{\partial^2 \theta}{\partial Y^2}\right) \tag{17}$$

where the modified Rayleigh number is:

$$\mathrm{Ra} = \frac{g\beta\Delta T L_H^3}{\nu\alpha} = \frac{g q_H L_H^4}{T_C k \nu\alpha} \tag{18}$$

The dimensionless velocity boundary conditions are $U_X = U_Y = 0$ at all walls. The dimensionless thermal boundary conditions are established by prescribed values of $\theta = 0$ at the inclined wall, $\partial\theta/\partial X = -1$ at the vertical wall and $\partial\theta/\partial Y = 0$ at the top adiabatic wall.

In view of the foregoing, the velocity field $U_X(X, Y)$, $U_Y(X, Y)$, and the temperature field $\theta(X, Y)$ are controlled by the aperture angle, φ, the modified Rayleigh and Prandtl numbers.

Computational procedure

The set of coupled governing equations and boundary conditions were solved numerically using the commercial finite element code, COMSOL Multiphysics version 3.5 [15] in conjunction with the numerical solver UMFPACK [16]. Three computational meshes consisting of roughly 2400, 6300, and 10300 triangular elements were tested to make a decision with regards to the optimal grid size. In all cases care was taken to increase the element density in vulnerable areas where high velocity and temperature gradients would occur, such as near the walls and vertices.

Table 1 shows the results of the grid sensitivity analysis for a critical case corresponding to the widest aperture angle ($\varphi = 45^o$) and the highest modified Ra = 10^9. Important parameters such as the maximum dimensionless velocity and temperature values and the Nusselt numbers at the hot vertical wall are reported. It can be seen that numbers listed in tab. 1 are similar and no appreciable differences (lower than 0.1%) are found when increasing the grid size from 6300 to 10300. As a result, in this work a mesh consisting of roughly 6300 triangular elements was chosen to carry out the totality of numerical computations involving suitable combinations of $\varphi \leq 45^o$ and $\mathrm{Ra} \leq 10^9$.

Table 1. Grid sensitivity for the widest triangular cavity with $\varphi = 45^{\circ}$ and the highest Ra = 10^9 (Pr = 0.72)

Number of elements	U_{max}	Nu_1	Nu_2
2404	$4.44 \cdot 10^{-2}$	14.89	29.32
6304	$4.32 \cdot 10^{-2}$	14.86	29.33
10334	$4.32 \cdot 10^{-2}$	14.86	29.33

For completeness, the computed results were validated against experimental results in previous works [9] for the same geometry but with a prescribed high temperature boundary condition at the vertical wall.

Results and discussion

Results are reported for the velocity (U_X, U_Y) and temperature, θ, fields as well as the Nusselt numbers at the hot vertical wall, based on the maximum and average hot wall temperature. In this paper, numerical results are reported for three different aperture angles $\varphi = 15^{\circ}$, 30°, and 45° and height-based modified Rayleigh numbers that range from a low Ra = 0 (pure conduction) to a high Ra = 10^9. It should be noted that the modified Rayleigh number is based on the idea that the temperature changes existing in the flow are of the order given by eq. (8). Once the numerical simulations were performed, it was confirmed that the temperature differences were much lower, which results in a difference of approximately two orders of magnitude in case the Rayleigh number is based on the actual maximum temperature difference.

All numerical computations were performed for air at standard atmospheric pressure. The cold wall temperature, T_C, and the uniform heat flux along the hot wall, q_H, were set to fixed values of 287 K and 20 W/m^2, respectively. Perfect gas behavior was assumed, so the thermal expansion coefficient, β, is given by $1/T_C$. The thermophysical properties of the fluid were assumed constant and, initially, equal to those for dry air evaluated at the cold wall temperature, T_C, using the code REFPROP [17]. Consequently, all the numerical computations share a same Prandtl number (Pr = 0.72), so for a given aperture angle, φ, the velocity and temperature fields are solely controlled by the modified Rayleigh number. However, a brief analysis of the possible effect of the Prandtl number appears as an addendum in the final section of the paper.

For a given geometry (defined by the aperture angle and cavity height) and fixed values of the heat flux and cold wall temperature, the modified Rayleigh number was controlled through the variation of the gravitational constant, g. In particular, the extreme case for g = 0 corresponds to the limiting conduction regime, *i. e.*, Ra = 0.

Velocity and temperature fields

Figure 2(a) shows the velocity streamlines for the air flow in 15°, 30°, and 45° triangular cavities induced by a low Ra = 10^3. The maximum values of the dimensionless velocity for the three cavities are listed in tab. 2. Dimensional values for a case relevant in practical electronic cooling applications are also included [18]. Results show that the velocity field (for the three configurations) exhibits a single clockwise rotating vortex, which takes the shape of the cavity. The vortex moves the warm fluid from the left vertical hot wall along the top insulated wall of the cavity and then comes down along the cold inclined wall. It is also seen that the velocity field approaches zero at the bounding walls. Even though the shape of the velocity field is qualitatively similar for the three cavities, two important differences are observed when increasing the cavity aperture angle from the slender 15° to the wide 45° cavity: the vortex continually moves down towards the center of the cavity. As a consequence, the maximum value of the dimensionless velocity, U_{max}, increases.

Table 2. Maximum dimensionless velocity and temperature values for the three cavities at Ra = 10^3, 10^6, and 10^8 (Pr = 0.72). Dimensional values for a practical application with T_C = 298 K and L_H = 0.1 m (g = 9.81 ms^{-2})

φ	Ra	U_{max}	θ_{max}	u_{max} (m·s^{-1})	T_{max} (K)
15º	10^3	$2.61\cdot10^{-3}$	0.220	$1.50\cdot10^{-5}$	298
	10^6	$5.12\cdot10^{-2}$	0.228	$9.32\cdot10^{-3}$	300
	10^8	$5.09\cdot10^{-2}$	0.107	$9.26\cdot10^{-2}$	406
30º	10^3	$1.05\cdot10^{-2}$	0.381	$6.04\cdot10^{-5}$	298
	10^6	$7.34\cdot10^{-2}$	0.262	$1.34\cdot10^{-2}$	301
	10^8	$5.07\cdot10^{-2}$	0.110	$9.23\cdot10^{-2}$	409
45º	10^3	$2.67\cdot10^{-2}$	0.508	$1.54\cdot10^{-4}$	298
	10^6	$7.55\cdot10^{-2}$	0.268	$1.37\cdot10^{-2}$	301
	10^8	$5.27\cdot10^{-2}$	0.108	$9.59\cdot10^{-2}$	407

The similarity picture obtained for the velocity field in the three cavities entails that a similar temperature field should also be obtained, which is confirmed in the isotherms represented in fig. 2(b). It can be seen that the main orientation of the temperature isotherms is vertical which signifies that, for the low modified Rayleigh number, the process is primarily dominated by conduction. The minimum temperature is obtained along the cold inclined wall, θ_{min} = 0, whereas the maximum temperature, θ_{max}, occurs always at the upper edge of the heated vertical wall. This trend should be expected, since the separation between the heated wall and the cold wall grows gradually from the bottom to the top of the cavity. It can also be observed that the isotherms are normal to the top insulated wall, in harmony with the imposed adiabatic boundary condition.

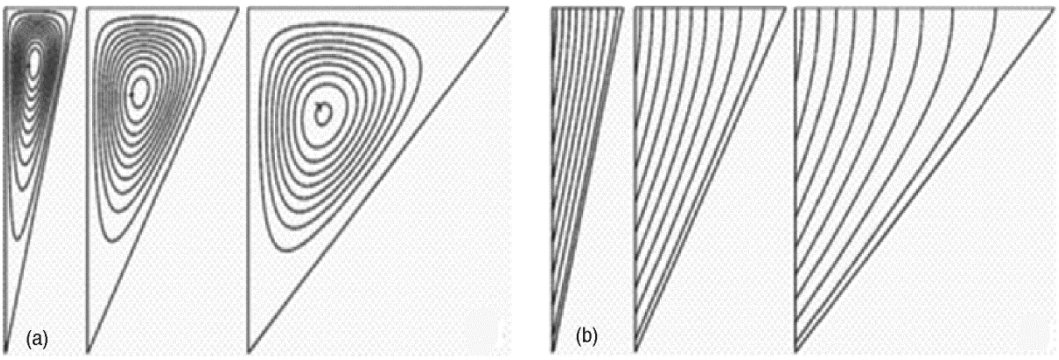

Figure 2. Streamlines (a) and isotherms (b) at Ra = 10^3 for the three aperture angles (φ) 15º, 30º, and 45º ($\Delta\theta = \theta_{max}/10$)

Table 2 also includes the numerical results for θ_{max} for the three triangular cavities, as well as the corresponding dimensional values for a practical application. The maximum dimensionless temperature increases considerably when the aperture angle is augmented from 15º to 45º. In numbers, for φ = 15º a value of θ_{max} = 0.220 is obtained. However, for the 45º cavity the dimensionless temperature shoots up to a value of θ_{max} = 0.508; more than a two-fold factor. This behavior must be attributed to an increased conductive heat transfer related to the small separation between the hot and cold walls for the slimmer configurations rather than to an almost imperceptible convective contribution.

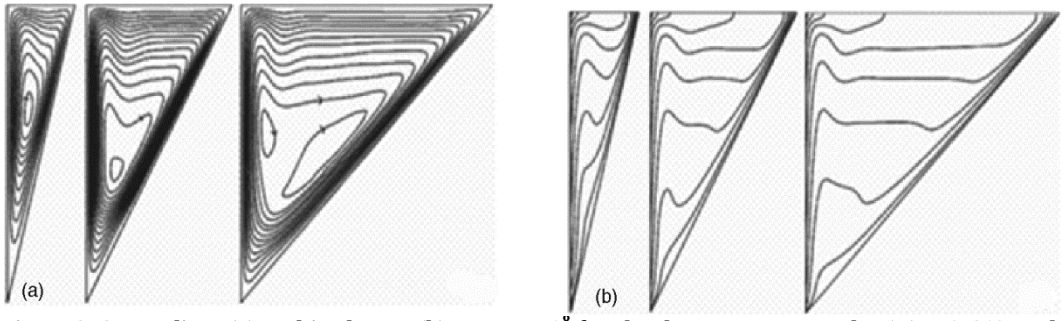

Figure 3. Streamlines (a) and isotherms (b) at Ra = 10^8 for the three aperture angles (φ) 15º, 30º, and 45º ($\Delta\theta = \theta_{max}/10$)

Figure 3 illustrates the same patterns but for a high Ra = 10^8. When comparing the streamlines of the cavities in fig. 3(a) with those in fig. 2(a), it is clear that the vortices have moved to the bottom of the cavity. Similar to the Ra = 10^3 case, the velocity field for the 15º and 30º cavities contains a single clockwise rotating vortex, which takes the shape of the cavity. However, it can be seen that the higher separation between the hot and cold walls for the wider 45º cavity configuration produces that the single vortex, that prevails near the cavity walls, splits into two smaller ones in the center of the cavity.

From the values of U_{max} collected in tab. 2 it is evident that the velocity values are increased significantly when compared against those for the Ra = 10^3 case. This increment in the velocity field translates into the fluid flow being now dominated by natural convection. Figure 3(b) clearly shows that individual thermal boundary layers develop along the vertical hot wall and the cold inclined wall because of the natural convection. However the development of the boundary layer is hindered by the presence of the top adiabatic wall. As a consequence, the boundary layer becomes much thicker and a thermally stratification region develops in the core of the cavity, where the isotherms are arranged horizontally instead of vertically. Since higher velocities are obtained, a more effective heat transfer is expected, which is confirmed by the lower maximum temperature values along the hot vertical wall, tab. 2. However, it should be noted that under these conditions the maximum dimensionless temperature is nearly invariant with the shape of the cavity.

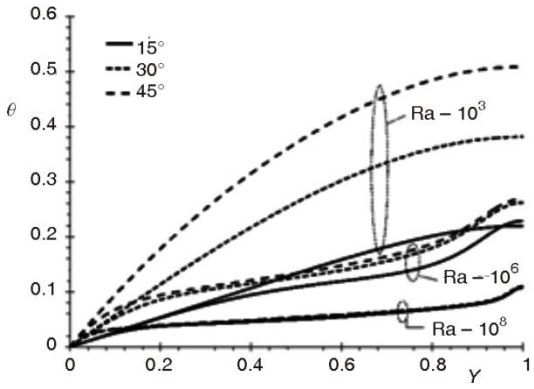

Figure 4. Dimensionless temperature profiles along the heated vertical wall at various Ra = 10^3, 10^6, and 10^8 for the three aperture angles (φ) 15º, 30º and 45º

To have a clearer map of the temperature field, the temperature profiles along the hot vertical wall are scrutinized for the cases considered previously. In fig. 4, the dimensionless temperature along the hot wall is plotted for a low Ra = 10^3, intermediate Ra = 10^6 and high Ra = 10^8 values, in association with the 15º, 30º, and 45º cavities. Focusing on the Ra = 10^3 case, it is clear that the heated wall temperature decreases considerably with decreasing aperture angles, φ. It can also be seen that the dimensionless temperature increases with a nearly constant slope, except in the vicinity of the upper edge where the

temperature profile changes smoothly to a zero slope value (in harmony with the top wall adiabatic boundary condition). For the intermediate Ra = 10^6 case, it is also observed that the dimensionless temperature increases with the aperture angle φ, though two main differences are palpable with respect to the results related to Ra = 10^3. The first main difference is that the temperature profiles for the three cavities are closer than for the Ra = 10^3 case, especially between the 30 and 45º configurations. The second main difference is that, now, the temperature profiles present a nearly constant and gently slope along the middle part of the wall, but abrupt temperature changes near the edges. In addition, it can be seen that the slope of the dimensionless temperature along the heated vertical wall ($\partial\theta/\partial Y|_{X=0}$) is lower for the Ra = 10^6 case than for the Ra = 10^3case in the vicinities of the bottom edge of the cavity, but higher near the upper edge. Finally, for the highest Ra = 10^8 case tested, the temperature profiles are nearly coincident for the three cavities and lower than for the previous Rayleigh number cases.

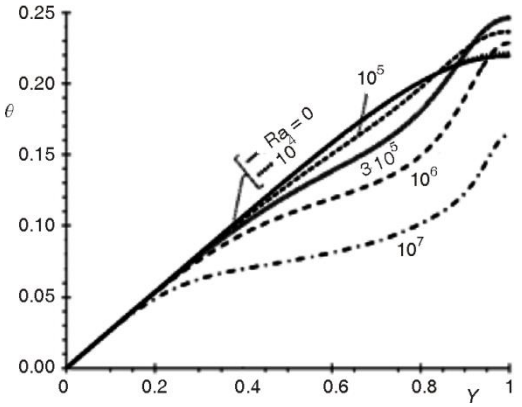

Figure 5. Dimensionless temperature profiles along the heated vertical wall at different modified Rayleigh numbers for the φ = 15º cavity

A closer look at the results shown in fig. 4, for the slender 15º cavity, reveals that the maximum vertical wall temperature (which occurs at the top vertex of the wall) is the highest for the intermediate Ra = 10^6 case, tab. 2. This behavior can be explained better with help from the results shown in figs. 5 and 6 for the 15º cavity. Shown in fig. 5 are the dimensionless temperature profiles, θ, along the vertical wall, Y, for selected values of Rayleigh number; whereas fig. 6 displays the corresponding numerical results of the Y-component of the dimensionless temperature gradient ($\partial\theta/\partial Y|_{X=0}$). For low Ra < 10^4 values, the velocity field is so weak that the effect of Rayleigh number on the heated wall temperature profiles is insignificant. For higher modified Rayleigh values (Ra > 10^4) it can be seen that, far down from the upper edge of the wall, the values of θ and $\partial\theta/\partial Y|_{X=0}$ decrease with increments in Rayleigh number, as a consequence of an increasing natural convective contribution that results from higher upward air velocities along the vertical wall. However, due to the buoyancy forces, the hot air tends to accumulate at the left-upper edge of the cavity hindering the cooling of the heated vertical wall. As a result a minimum value for $\partial\theta/\partial Y|_{X=0}$ is reached for an intermediate value of the dimensionless vertical position, Y. Up from this point, θ, increases more rapidly along the vertical wall ($\partial\theta/\partial Y|_{X=0}$increases) with higher values of the modified Rayleigh number. Finally, close to the upper edge of the wall a maximum value for $\partial\theta/\partial Y|_{X=0}$ is attained to become of null

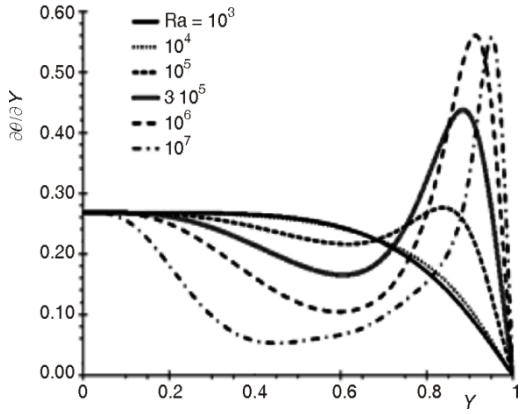

Figure 6. Y-component of the dimensionless temperature gradient along the heated vertical wall ($\partial\theta/\partial Y|_{X=0}$) at different modified Rayleigh numbers for the φ = 15º cavity

value at the upper edge of the wall ($\partial\theta/\partial Y|_{X=0,Y=1} = 0$). The previous mentioned tendencies are more pronounced with elevations in the modified Rayleigh number.

In summary, the numerical results in fig. 6 demonstrate that when the modified Rayleigh number grows, this produces two opposite effects. On the one hand the air velocity increases, favoring the cooling of the lower portion of the heated vertical wall. On the other hand the heated air raises to the top-left corner of the cavity where nearly stagnant fluid regions exist, hindering the heat removal from the upper region of the vertical wall. The final result that emerges from the combination of these opposite effects can be seen in fig. 5; that is, in the low Rayleigh range ($0 \leq \mathrm{Ra} \leq 3\cdot10^5$), an unexpected (a priori) heat transfer deterioration is found with incremental values of Rayleigh number. This deterioration finds its maximum for a modified Rayleigh number of $\mathrm{Ra}_{crit} = 3\cdot10^5$ which holds a dimensionless temperature at the upper edge of $\theta_{max} = 0.246$, representing an increment of around 12% with respect to the limiting pure conduction case at Ra = 0 ($\theta_{max} = 0.219$). For Rayleigh values higher than Ra_{crit}, the dimensionless wall temperature decays rapidly with Rayleigh number, as expected. The heat transfer deterioration phenomenon was also observed for the other 30º and 45º cavities, though the values of Ra_{crit} are slightly different.

Heat transfer features

For the purpose of numerically analyzing the heat transfer features of the cavity the Nusselt numbers along the vertical walls are calculated:

$$\mathrm{Nu}(Y) = \frac{q_H L_H}{k\left[T(Y) - T_C\right]} = \frac{1}{\theta(Y)} \tag{19}$$

Two different Nusselt numbers are evaluated. The first one is the minimum Nusselt number along the hot wall, Nu_1, which is readily determined from the maximum temperature along the hot vertical wall, and given by:

$$\mathrm{Nu}_1 = \mathrm{Nu}(Y=1) = \frac{1}{\theta_{max}} \tag{20}$$

The second is the mean Nusselt number, Nu_2, given by:

$$\mathrm{Nu}_2 = \frac{1}{\overline{\theta}(Y)} = \frac{1}{\int_0^1 \theta(Y)\mathrm{d}Y} \tag{21}$$

The minimum Nusselt numbers, Nu_1, are plotted in fig. 7 as a function of the modified Rayleigh number for the three aperture angles analyzed (15º, 30º, and 45º). Numerical results indicate that for low Rayleigh numbers, the Nusselt number decreases softly with the modified Rayleigh number for the three aperture angles. This deterioration in the heat transfer behavior was already explained in the section *Velocity and temperature fields* and is maintained until a critical modified Rayleigh number, Ra_{crit}, is reached (which is represented by filled black symbols in fig. 7). For modified Rayleigh values higher than Ra_{crit}, the Nusselt number shoots up with increasing values of Rayleigh number for the three aperture angles. Then, taking into account the gently dependency of Nusselt number with Rayleigh number for $\mathrm{Ra} < \mathrm{Ra}_{crit}$ when compared with that for $\mathrm{Ra} > \mathrm{Ra}_{crit}$, the critical modified Rayleigh number may be also considered as the modified Rayleigh value that marks the demarcation point between the conduction and convection heat transfer modes. Also fig. 7 reveals that the critical modified Rayleigh number augments when the aperture angle diminishes.

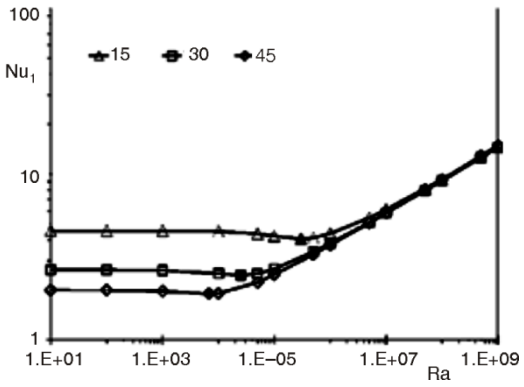

Figure 7. Variation of the minimum Nusselt number with the modified Rayleigh number for the three aperture angles 15º, 30º, and 45º (Solid filled points represent results for Ra = Ra_{crit})

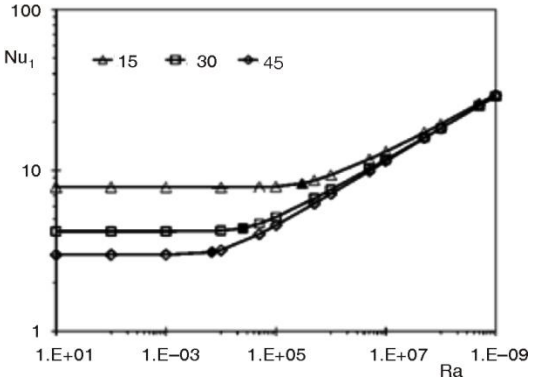

Figure 8. Variation of the mean Nusselt number with the modified Rayleigh number for the three aperture angles 15º, 30º, and 45º (Solid filled points represent results for Ra = Ra_{crit})

Upon comparing the results for the three aperture angles reflects that when the aperture angle is drastically reduced from 45º to 15º, the minimum Nusselt number, Nu_1, ascends remarkably in the low $Ra < Ra_{crit}$ range. However, for values of the modified Rayleigh number higher than Ra_{crit}, the Nu_1 curves for the three cavities tend to overlap and merge into a single curve. In essence, this means that from the point of view of controlling the wall temperatures (controlling the maximum or critical temperature) the three cavities perform similarly once the modified Rayleigh value is high enough to guarantee that the convective heat transfer mode is dominant.

Plotted in fig. 8 is the same set of results delineated before, but for the mean Nusselt number, Nu_2, instead. An analysis of the curves in fig. 8 leads to similar conclusions that those sustained for fig. 7. However, now, for $Ra < Ra_{crit}$, the Nusselt number elevates softly with the modified Rayleigh number for the three aperture angles. Since Nu_2 is based on the hot wall average temperature rather than on the maximum or critical temperature, the values of Nu_2 are higher than Nu_1 by a factor between 1.5 and 2.

Table 3. Effect of the Prandtl number on the heat transfer features for the widest triangular cavity with $\varphi = 45^o$ at Ra = 10^3, 10^6, and 10^8

Pr	Ra	Nu_1	Nu_2
0.25	10^3	1.97	3.00
	10^6	3.67	6.96
	10^8	8.93	18.50
0.50	10^3	1.97	3.00
	10^6	3.72	7.12
	10^8	9.24	18.17
0.72	10^3	1.97	3.00
	10^6	3.73	7.17
	10^8	9.27	18.35
1	10^3	1.97	3.00
	10^6	3.73	7.20
	10^8	9.22	18.46

Effect of the Prandtl number

The previous results shared a common Prandtl number of Pr = 0.72, which corresponds to air at a temperature equal to T_C and standard atmospheric pressure. It is well known that, for air as well as many gases, typical values of the Prandtl number are around 0.6 to 0.8. However, in order to visualize the effect of the Prandtl number, additional computations were also performed for three Prandtl numbers of 0.25 and 0.5 (binary gas mixtures) and 1 (vapors), for the widest cavity size, $\varphi = 45$. In tab. 3, the numerical results of these computations are collected and compared with those for Pr = 0.72. It can

be recognized that the minimum and average Nusselt numbers are almost invariant with Prandtl number, producing maximum deviations (with respect to the baseline value for Pr = 0.72) of 3.8% for the relatively low Pr = 0.25 case. Therefore, results of this paper can be safely used by those analysts that employ binary mixtures of gases as working fluids for cooling.

Conclusions

In this paper the problem of natural convection in a right-angled triangular cavity filled with air has been analyzed from the perspective of thermal boundary conditions. A prescribed heat flux was imposed to the vertical wall, a prescribed cold temperature was assigned at the inclined wall and the upper horizontal wall was assumed thermally insulated. Using the finite element method, the analysis was performed for height-based modified Rayleigh numbers that range from a low Ra = 0 (pure conduction) to a high Ra = 109 (vigorous natural convection) in conjunction with the three aperture angles of 45º, 30º, and 15º. The numerical computations were channeled through the determination of the minimum Nusselt number, Nu_1, and a mean Nusselt number, Nu_2, along the hot vertical wall, both are based on the maximum and mean temperatures along the hot vertical wall, respectively.

The following major conclusions are drawn from the detailed analysis of the numerical results.

- For all suitable combinations of the height-based modified Rayleigh number and aperture angle, as expected the maximum temperature occurs always at the upper edge of the heated vertical wall.
- A critical modified Rayleigh number exists that marks the threshold between the conduction mode and the natural convection mode. The value of the critical Rayleigh number decreases for higher aperture angles.
- For all configurations Nu_2 increases with increments in Rayleigh number, *i. e.*, the mean temperature along the hot wall decreases with Rayleigh number.
- For all configurations Nu_1 increases with increments in Rayleigh number when $Ra > Ra_{crit}$, whereas Nu_1 decreases with Rayleigh number for $Ra < Ra_{crit}$. This means that a heat transfer deterioration surfaces up with increasing values of Rayleigh number in the low Rayleigh range ($Ra < Ra_{crit}$), *i. e.*, higher values of the maximum wall temperature are attained.
- For low modified Rayleigh numbers the thermal performance (Nu_1 and Nu_2) improves for lower aperture angles. This behavior must be attributed to an increased conductive heat transfer related to the small separation between the hot vertical and cold inclined walls.
- In contrast, for high modified Rayleigh numbers, the thermal performance is merely equal for the three aperture angles studied. Then, the same value of the maximum or critical temperature along the hot vertical wall is prevalent.

Nomenclature

g – gravitational acceleration, [ms^{-2}]
k – thermal conductivity, [Wm^{-1}K^{-1}]
L – length of wall, [m]
Nu – Nusselt number, $\{= q_H L_H/[k(T-T_C)]\}$ [–]
Nu_1 – minimum Nusselt number along the hot vertical wall
Nu_2 – mean Nusselt number along the hot vertical wall
P – pressure, [Pa]
Pr – Prandtl number, $[= \upsilon/\alpha]$ [–]
p – dimensionless pressure, $p/(\rho V_c^2)$ [–]
q – heat flux, [Wm^{-2}]

Ra – modified Rayleigh number, [= $gq_H L_H^4/(\alpha\upsilon kT_C)$] [–]
s – distance along a wall measured from the bottom vertex, [m]
T – absolute temperature, [K]
ΔT – temperature differences in the fluid, [K]
U – dimensionless velocity, (= u/V_c) [–]
u – velocity, [ms^{-1}]
V_c – characteristic velocity, eq. (10), [ms^{-1}]
X, Y – dimensionless Cartesian co-ordinates, x/L_H, y/L_H, [–]
x, y – Cartesian co-ordinates, [m]

Greek symbols

α – thermal diffusivity, [m^{2}s^{-1}]
β – coefficient of volumetric thermal expansion, [K^{-1}]
θ – dimensionless temperature, [$=(T-T_C)/(q_H \cdot L_H/k)$] [–]
μ – dynamic viscosity, [kgm^{-1}s^{-1}]
υ – kinematic viscosity, [m^{2}s^{-1}]
ρ – density, [kgm^{-3}]
φ – aperture angle, [°]

Subscripts

A – adiabatic
C – cold
cri – critical
H – hot
w – wall surface
x, y – components in the x- and y-directions
X, Y – dimensionless x, y

References

[1] Incropera, F., DeWitt, D. P., *Introduction to Heat Transfer*, 4th ed., John Wiley and Sons, Hoboken, N. J., USA, 2002, pp. 524-530
[2] Cengel, Y. A., *Heat Transfer: A Practical Approach*, 2nd ed., McGraw-Hill, New York, USA, 2003, pp. 477-486
[3] Raithby, G. D., Hollands, K. G. T., Natural Convection, in: *Handbook of Heat Transfer* (Eds. W. M. Rohsenow, J. Hartnett, Y. Cho), 3rd ed., Mc Graw-Hill, New York, USA, 1998
[4] Jaluria, Y., Natural Convection, in: *Heat Transfer Handbook* (Eds. A. Bejan, A. D. Kraus), John Wiley and Son, New York, USA, 2003
[5] Holtzman, G. A., *et al*., Laminar Natural Convection in Isosceles Triangular Enclosures Heated from Below and Symmetrically Cooled from Above, *Journal of Heat Transfer*, *122* (2000), 3, pp. 485-491
[6] Del Campo, E. M., *et al*., Analysis of Laminar Convection in a Triangular Enclosure, *Numerical Heat Transfer, Part A, 13* (1988), 3, pp. 353-372
[7] Elicer-Cortes, J. C., Kim-Son, D., Natural Convection in a Dihedral Cavity: Influence of the Angle and the Temperature of the Walls on the Mean Thermal Field, *Experimental Heat Transfer*, *6* (1993), 3, pp. 205-213
[8] Ridouane, E. H., *et al*., Natural Convection Patterns in Right-Angled Triangular Cavities with Heated Vertical Sides and Cooled Hypotenuses, *Journal of Heat Transfer*, *127* (2005), 10, pp. 1181-1186
[9] Sieres, J., *et al*., Effect of Surface Radiation on Buoyant Convection in Vertical Triangular Cavities with Variable Aperture Angles, *International Journal of Heat and Mass Transfer*, *50* (2007), 25-26, pp. 5139-5149
[10] Saha, S. C., Khan, M. M. K., A Review of Natural Convection and Heat Transfer in Attic-Shaped Space, *Energy and Buildings*, *43* (2011), 10, pp. 2564-2571
[11] Kaluri, R. S., *et al*., Bejan's Heatline Analysis of Natural Convection in Right-Angled Triangular Enclosures: Effects of Aspect-Ratio and Thermal Boundary Conditions, *International Journal of Thermal Sciences*, *49* (2010), 9, pp. 1576-1592
[12] Simons, R. E., *et al*., Heat Transfer in Electronic Packages, in: *Microelectronics Packaging Handbook* (Eds. R. R. Tummala, E. J. Rymaszewski, A. G. Klopfenstein), 2nd ed., Chapman and Hall, New York, USA, 1997, pp. 315-403
[13] Bar-Cohen, A., *et al*., Heat Transfer in Electronic Equipment, in: *Heat Transfer Handbook* (Eds. A. Bejan, A. D. Kraus), John Wiley and Son, New York, USA, 2003
[14] Chu, R. C., The Challenges of Electronic Cooling: Past, Current and Future, *Journal of Electronic Packaging*, *126* (2004), 4, pp. 491-500
[15] ***, COMSOL, Inc., COMSOL MultiphysicsUser's Guide, Version 3.5, Burlington, Mass., USA, 2008
[16] Davis, T. A., Algorithm 832: UMFPACK V4.3-An Unsymmetric-Pattern Multifrontal Method, *ACM Transactions on Mathematical Software*, 30 (2004), 2, pp. 196-199

[17] Lemmon, E. W., *et al*., *NIST Standard Reference Database 23: Reference Fluid Thermodynamic and Transport Properties-REFPROP*, Version 9.0. National Institute of Standards and Technology, Standard Reference Data Program, Gaithersburg, Md., USA, 2010
[18] Wang, Z., Mayinger, F., Natural Convection Heat Transfer in the PCB's Array of Electronic Equipments, *Proceedings* (Ed. B. Sunden), 1st Baltic Heat Transfer Conference, Gotenburg, Sweden, 1991, pp. 841-854

Paper submitted: May 30, 2013
Paper revised: January 28, 2014
Paper accepted: February 24, 2014